Atmos. Meas. Tech. Discuss., 7, 6699–6742, 2014
www.atmos-meas-tech-discuss.net/7/6699/2014/
doi:10.5194/amtd-7-6699-2014

Atmospheric Measurement Techniques Discussions
Open Access

An improved retrieval of tropospheric NO_2 from space over polluted regions using an earthshine reference

J. S. Anand, P. S. Monks, and R. J. Leigh

Earth Observation Science, Department of Physics and Astronomy, University of Leicester, Leicester, LE1 7RH, UK

Received: 8 May 2014 – Accepted: 14 June 2014 – Published: 10 July 2014

Correspondence to: R. J. Leigh (rl40@le.ac.uk)

Published by Copernicus Publications on behalf of the European Geosciences Union.

Abstract

A novel tropospheric NO_2 DOAS retrieval algorithm optimised for a nadir-viewing satellite instrument imaging polluted areas is proposed in this work. Current satellite DOAS retrievals have relied on using a solar reference spectrum to derive a total slant column, then using either model assimilation or spatial filtering to derive the tropospheric component. In the ESrs-DOAS (EarthShine reference sector DOAS) algorithm, tropospheric NO_2 slant columns are derived using spectra averaged from measurements over unpolluted regions, thus removing the need for a solar reference spectrum, though some residual stratospheric signal still has to be removed. To validate the ESrs-DOAS algorithm, DOAS retrievals were performed on modelled spectra created by the radiative transfer model- SCIATRAN, as well as L1B earthshine radiance data measured by the NASA/KNMI Ozone Monitoring Instrument (OMI). It was found that retrievals using an earthshine reference produce spatial distributions of tropospheric NO_2 over eastern China during June 2005 that highly correlate with those derived using existing retrieval algorithms. Comparisons with slant columns retrieved by the operational NO_2 retrieval algorithm for OMI (OMNO2A) show that the ESrs-DOAS algorithm greatly reduces the presence of artificial across-track biases (stripes) caused by calibration errors, resulting in a 27 % reduction in retrieval uncertainty. The ESrs-DOAS technique also reveals absorption features over the Sahara and similar regions characteristic of sand absorption, as first discovered in analysis of GOME-2 NO_2 retrievals. Potentially, future satellite instruments optimised for using the ESrs-DOAS algorithm would not need a solar reference, which would simplify their optical and mission design.

1 Background

Anthropogenic emissions of nitrogen dioxide (NO_2) have been associated with poor health in urban areas; both as a direct contributor to respiratory conditions and as a source of secondary pollutants such as nitric acid (WHO, 2003). Additionally,

AMTD
7, 6699–6742, 2014

tropospheric NO_2 through photolysis contributes to tropospheric ozone (O_3) production (Chameides et al., 1992). A significant proportion of NO_2 also exists in the stratosphere, where it is active in processes involved in the creation and destruction of O_3 (Wayne, 1991).

Since the launch of the GOME instrument in 1996 (Burrows et al., 1999) satellite instruments have been employed to retrieve global tropospheric NO_2 concentrations from earthshine radiance spectra. The NO_2 vertical column densities (VCDs) derived from these measurements have been used for a range of applications (Monks and Beirle, 2011), such as determining pollution trends over megacities (e.g. Konovalov et al., 2010), shipping emissions (e.g. Richter et al., 2004), and to validate air quality models (e.g. Huijnen et al., 2010). Validation of tropospheric NO_2 VCDs from these retrievals are primarily performed through intercomparison campaigns with ground-based or airborne instruments during satellite overpasses. During an overpass the satellite derived tropospheric NO_2 VCDs are compared with those derived by the ground based instruments in the ground pixel. Measurements of the ambient NO_2 and aerosol profile are also used to validate the a priori information used in the satellite VCD calculation (e.g. Hains et al., 2010). However, biases arising from factors such as ground pixel coverage need to be accounted for in order to accurately quantify the precision of the retrieval.

A significant issue in retrieving tropospheric NO_2 from space is that of separating the tropospheric NO_2 VCD from the background stratospheric contribution, which can be a significant source of error (Boersma et al., 2004). In order to remove the presence of stratospheric NO_2 previous retrieval algorithms have relied on either spatial filtering of averaged data (e.g. Bucsela et al., 2006), or through model assimilation (e.g. Boersma et al., 2007).

In the case of some push-broom instruments (e.g. OMI, Levelt et al., 2006) the retrieved slant columns also exhibit non-physical "stripes", which result from across-track biases caused by slight differences in wavelength calibration between adjacent viewing angles. These biases need to be removed by spatial filtering over several adjacent swaths.

AMTD
7, 6699–6742, 2014

An implicit part of the DOAS retreivals from these UV/VIS instruments is that the reference spectrum is normally a solar irradiance spectrum, used as a measure of the incoming radiation before attenuation by the atmosphere. One possible alternative would be to use earthshine radiance spectra recorded over an unpolluted region as a reference. This type of technique has previously been employed in several DOAS retrievals of trace gases such as IO (Schönhardt et al., 2008) and HCHO (De Smedt et al., 2008). In both cases averaged earthshine radiance spectra over the remote Pacific were used, as the background concentration of these gases are expected to be relatively low in that region. Using an earthshine reference spectrum is advantageous, in that it also reduces residual instrument noise occurring from differences between spectra measured during the instrument's solar and terrestrial viewing modes. In addition, the technique helps to cancel out the impact the Ring effect (Chance and Spurr, 1997) has on the retrieval, as the radiance spectra has already been subject to some Ring absorption (Schönhardt et al., 2008).

The objective of this work is to determine whether the tropospheric NO_2 SCD can be directly retrieved using an unpolluted earthshine radiance (the "ESrs-DOAS" technique) with a reduced need for model assimilation or spatial filtering, and to evaluate any practical benefits that arise from doing so. If such benefits exist, then future NO_2 spectrometer designs would be greatly simplified without the need to measure a solar irradiance reference spectrum.

1.1 Differential Optical Absorption Spectroscopy (DOAS)

In general, UV/VIS NO_2 retrieval algorithms for spectra from grating spectrometers (e.g. Richter and Burrows, 2002; Sierk et al., 2006; Bucsela et al., 2006) have used the DOAS technique (Platt and Stutz, 2006) to retrieve slant column densities (SCDs). In the absence of multiple scattering these can be considered to be the integrated trace gas density along the instrument's geometrical line of sight. The technique is based on the principle that a wavelength dependent absorption signal can be split into two components; the low frequency, broadband component (representative of features such

AMTD
7, 6699–6742, 2014

as aerosol scattering and surface albedo) that can be approximated by a low-order polynomial, and a high frequency component that is sensitive to trace gas concentrations. In principle the DOAS fit is a non-linear least squares fit of the logarithm of the reflectance spectrum (the ratio of the incident and attenuated spectra) over a given wavelength range, using a modified form of the Beer–Lambert Law:

$$\ln\left(\frac{I(\lambda)}{I_0(\lambda)}\right) = -\sum_i \sigma_i(\lambda)\mathrm{SCD}_i + P(\lambda) \quad (1)$$

In Eq. (1) the reference and object spectra are represented by I_0 and I respectively. For satellite retrievals of NO_2 I would be the measured earthshine radiance spectra, while solar irradiance spectra measured separately by the instrument would be used as I_0. In this case the retrieved SCD would be the total slant column density along the line of sight.

σ_i represents the absorption cross section of the ith trace gas considered in this fit, while P represents the low-order polynomial used to account for the broadband structure in the spectra. Ideally, the trace gas absorption cross sections and wavelength ranges considered in the fit should be such that the cross sections are orthogonal to each other to give the best result, though in practice this often does not occur, and can be a large source of error in the fit.

In previous retrievals of NO_2 the wavelength range considered for the DOAS fit has typically been within the 400–500 nm band. Additionally, trace gas absorption cross sections such as O_3, H_2O and the O_2-O_2 collision complex within this band have also been included in the fit to account for other sources of absorption in the spectra. Furthermore, a synthetic cross section to account for absorption caused by rotational Raman scattering (the Ring effect; Chance and Spurr, 1997) is also included in the fit.

SCDs retrieved by DOAS still need to be weighted in order to account for enhancement owing to factors such as optical path length, scattering from clouds/aerosols, and surface albedo. To that end, the SCDs are divided by an air mass factor (AMF) to convert them into VCDs (e.g. Boersma et al., 2004). The AMFs are in turn created by

AMTD
7, 6699–6742, 2014

inputting forward model parameters describing local conditions such as surface albedo, trace gas profile information and cloud cover into a radiative transport model (RTM). Quantifying the uncertainty in the forward model parameters is important for determining the final retrieval error of the derived VCDs Boersma et al. (2004).

1.2 The Ozone Monitoring Instrument (OMI)

Launched in 2004 onboard the NASA AURA satellite, the Ozone Monitoring Instrument (OMI, Levelt et al., 2006) produces tropospheric NO_2 VCDs at a near-urban spatial resolution (nadir pixel size: 13 km × 24 km, though in its' spatial zoom modes this can be reduced to 13 km × 12 km or even 13 km × 3 km, as discussed in Valin et al., 2011). As a push-broom spectrometer, OMI has a swath width of 2600 km which are divided into 60 across-track pixels. Each pixel corresponds to a separate viewing angle. OMI follows a sun-synchronous orbit, with a local equatorial overpass time of 13:45 LT. The instrument's visible channel has a 350–500 nm spectral range, with an average spectral resolution of 0.63 nm.

The process of deriving tropospheric NO_2 VCDs from the Level 1B earthshine radiance data (OML1BRVG product, see Method) via DOAS is described is briefly summarised in this section. In the operational OMI DOAS retrieval algorithm, OMNO2A (Bucsela et al., 2006, J. van Geffen, personal communication, 2013) the earthshine reflectance spectra is fitted using a 405–465 nm fitting window. The reflectance spectra is fitted with absorption cross-sections for NO_2, O_3 and H_2O, as well as a 5th order polynomial to account for broadband variations (see Table 1).

In the OMNO2A algorithm the Ring effect is treated differently compared with traditional DOAS retrievals. In this case the Ring effect is treated as a source of photons, rather than a pseudo-absorber. Because of this, the algorithm performs a nonlinear least squares fit using the following equation:

$$\left(\frac{I(\lambda)}{I_0(\lambda)}\right) = P(\lambda)\exp\left[\left(-\sum_i \sigma_i \mathrm{SCD}_i\right)\right] \times \left(1 + \frac{C_{\mathrm{RING}} I_{\mathrm{RING}}(\lambda)}{I_0(\lambda)}\right) \quad (2)$$

AMTD
7, 6699–6742, 2014

In Eq. (2) P represents a 5th order polynomial, while the I_{RING} term is the Ring radiance spectrum, and C_{RING} is the Ring absorption coefficient determined by the fit. In this case the Ring terms describe first the absorption through the photon path through the atmosphere before a scattering event occurs (the "1" term). The Ring radiance spectrum describes the filling in of the Fraunhofer lines that occurs only after the scattering event, and that these events occur as the photons are travelling towards the satellite.

There are currently three operational algorithms that process the SCDs retrieved by OMNO2A into tropospheric NO_2 VCDs; brief descriptions of each are discussed below.

1.2.1 Standard product (OMNO2, v 3.0, NASA)

After an initial geometric AMF is applied to the SCD, the stratospheric NO_2 VCD is estimated by first masking polluted regions and then applying planetary wave analysis over known unpolluted regions to compute the smoothly varying stratospheric background. After subtracting this component a tropospheric AMF is calculated using profile data from the Global Monitoring Initiative (GMI) Chemical Transport Model (CTM), along with scattering weights derived from the TOMS radiative transfer model (TOMRAD) and terrain albedo derived from OMI reflectance data (Kleipool et al., 2008). AMFs are weighted for cloud cover using cloud fraction data from the OMI O_2-O_2 cloud algorithm (OMCLDO2, Acarreta et al., 2004). See Bucsela et al. (2013, 2006) and Celarier et al. (2013) for more details.

1.2.2 Derivation of OMI tropospheric NO_2 product (DOMINO, v 2.0, KNMI)

In the DOMINO algorithm the stratospheric SCD is derived by assimilating the retrieved SCD in the TM4 global CTM (Boersma et al., 2007). As in the Standard Product, the resulting tropospheric VCD is calculated using an AMF using similar datasets for terrain albedo, and cloud fractions, while the NO_2 profiles and scattering weights are derived from TM4 model runs and the DAK radiative transfer (RTM) model. The assimilated

AMTD
7, 6699–6742, 2014

stratospheric NO_2 SCD has been validated by comparing assimilated data with independent ground based measurements (Dirksen et al., 2011). See Boersma et al. (2007, 2011) for more details.

1.2.3 Berkeley High-Resolution product (BEHR, Uni. of California, Berkeley)

The BEHR product relies on the stratospheric removal and initial VCD estimate retrieved by the Standard Product, and largely follows the same procedure as the other two algorithms. This algorithm uses higher resolution a priori data such as MODIS measurements of albedo averaged over the OMI ground pixel to derive the AMF. See Russell et al. (2011) for more details.

It has been previously noted that NO_2 VCDs retrieved by OMI show systematic enhancements over specific viewing angles ("stripes"). These stripes do not correspond to any known geophysical behaviour, and were found to be a result of a combination of solar diffusor features and noise in solar irradiance measurements (Veihelmann and Kleipool, 2006). These features result in slight differences in wavelength calibration between the 60 across-track pixels, which in turn result in unknown offsets in the DOAS fits. Therefore, these features need to be empirically corrected after the retrieval. In order to suppress these stripes the daily solar irradiance spectra used in the DOAS fit was instead replaced with a composite of all solar irradiance measurements during 2005. Additionally, current retrievals attempt to filter these defects by comparing the background NO_2 field over several adjacent orbits (Boersma et al., 2011; Celarier et al., 2008).

2 Method

The QDOAS software package (v 2.1, http://uv-vis.aeronomie.be/software/QDOAS/, last access: 1 October 2013, Fayt et al., 2013) was employed to perform the DOAS fits in this investigation. This software package has typically been used in the past

AMTD
7, 6699–6742, 2014

to process spectral data from ground-based and airborne observations (e.g. Vlemmix et al., 2011; Popp et al., 2012), as well as in retrievals using satellite data (e.g. Hewson et al., 2013). A summary of all absorption cross sections used in this paper is included in Table 1 and Fig. 2. As with the OMNO2A algorithm, the fitting window for all DOAS fits in this work is set to 405–465 nm in order to minimise absorption from H_2O and the Ring effect (Boersma et al., 2007).

2.1 Retrieval using modelled spectra

The goal of this first effort was to demonstrate the theoretical possibility of using an earthshine reference in the DOAS fit and show in the absence of noise, aerosol and trace gas contamination that the earthshine-retrieved SCD is the difference in NO_2 between the reference and observed region. In order to demonstrate the validity of using earthshine reference spectra to retrieve tropospheric NO_2, the SCIATRAN RTM (v 3.1.27 Rozanov et al., 2005) was used to simulate spectra that may typically be observed over the Pacific and China. Vertical profile data for temperature, NO_2, O_3 and H_2O in these scenarios was provided by the CAMELOT dataset (Veefkind, 2009) and are summarised in Fig. 1. The Pacific is relatively free of tropospheric NO_2, which theoretically makes it possible for spectra taken over this region to be used as an estimation of the local stratospheric field over a given location.

An earthshine radiance spectrum from the Pacific and polluted Chinese scenarios was modelled, with absorption due to O_2-O_2 provided by a profile created by SCIATRAN from the pressure profile. Absorption from the Ring effect was calculated by SCIATRAN using the algorithm developed by Vountas et al. (1998). While no aerosol information was included, the solar zenith angle in either scenario was varied between 0–80° in order to demonstrate the retrieval's accuracy at different diurnal ranges. DOAS fits were carried out on all spectra using the solar irradiance spectrum as a reference. For Chinese scenarios the Pacific earthshine spectrum was used as a reference as well.

AMTD
7, 6699–6742, 2014

2.2 Retrieval using OMI L1B spectral data

In order to test the validity of the ESrs-DOAS technique using operational satellite spectra, data from the OML1BRVG (v. 3.0, Van den Oord et al., 2006; Dobber et al., 2008a) product was used to provide the calibrated, wavelength-corrected spectra for both the reference and object spectra in the DOAS retrieval in this work. Data regarding the ground pixel quality (e.g. cloud cover, surface albedo) was provided by the DOMINO (v. 2.0) product. Tropospheric SCDs retrieved by DOMINO were used to compare with the retrieved NO_2, though these had to be reconstructed using the "TroposphericVerticalColumn" and "AirMassFactorTropospheric" fields in the DOMINO data product. Similarly, the tropospheric SCDs retrieved by OMNO2 were derived from the "ColumnAmountNO2Trop" and "AmfTrop" fields in the OMNO2 data product, while the OMNO2A total SCDs were taken from the "SlantColumnAmountNO2" field. For the most of this work only data collected before 2008 was considered, as this was largely before the emergence of the "row anomaly" artefacts that have affected OMI data coverage since 2007 (Braak, 2010). All cross-sections used were convolved with the OMI slit function prior to the DOAS fit (Dobber et al., 2005).

Prior to the DOAS fit, the reference spectrum is interpolated onto the same wavelength grid as the earthshine radiance spectrum using the same interpolation technique as used in Bucsela et al. (2006). The interpolated reference spectrum $I_{0,\lambda(\mathrm{ES})}$ is calculated using the following equation:

$$I_{0,\lambda(\mathrm{ES})} = I_{0,\lambda(\mathrm{REF})} \frac{F_{\lambda(\mathrm{REF})}}{F_{\lambda(\mathrm{ES})}} \tag{3}$$

First, a high resolution oversampled solar atlas that is convolved to the OMI instrument line shape (Dobber et al., 2008b) is interpolated onto both the reference and radiance spectra wavelength grids ($F_{\lambda(\mathrm{REF})}$ and $F_{\lambda(\mathrm{ES})}$ respectively) using cubic spline interpolation. The ratio of these interpolated spectra is then multiplied by the intensity of the solar irradiance, which therefore gives the desired interpolation.

AMTD
7, 6699–6742, 2014

A wavelength correction is applied to the earthshine spectra before the DOAS fit, in order to correct for shifts caused by cloudy scenes (Voors et al., 2006). The correction is performed as a single offset, calculated from comparing the 408–423 nm spectral window to the high resolution solar atlas (van Geffen, 2013, personal communication). The offsets applied for each OMI ground pixel can be found in the "WavelengthRegistrationCheck" field in the OMNO2 product. Additionally, spectral pixels flagged as being affected by instrumental defects such as random telegraph signals or dark current behaviour were removed prior to the DOAS fit (Van den Oord et al., 2006). In QDOAS this removal can be performed by specifying gaps in the spectral window which are then ignored in the analysis.

3 Results

3.1 ESrs-DOAS retrievals of modelled polluted Chinese spectra

The results from the ESrs-DOAS fits of modelled CAMELOT spectra (see Section: 2.1) are discussed herein. As shown in Fig. 3, for all solar zenith angles considered the SCD retrieved by DOAS fitting spectra from the Chinese scenario using a Pacific earthshine reference was near-identical to the difference in the modelled total SCD between the two scenarios. From Fig. 1 it appears that the difference in SCD is largely due to differences in tropospheric NO_2, though the difference in stratospheric NO_2 between the two scenarios would also greatly contribute to the retrieved SCD. Ideally, the reference spectra should be collected from a region where the stratospheric NO_2 is similar to the target region to minimise this bias.

3.2 Residual bias in QDOAS retrieval estimation using OMI spectra

Prior to comparing tropospheric SCDs in satellite data, it is essential to determine any inherent biases present in the retrieval algorithm, as QDOAS performs DOAS fits differently to OMNO2A. QDOAS performs a nonlinear DOAS fit by solving a variant

AMTD
7, 6699–6742, 2014

of Eq. (1), in which the Ring is treated as a pseudo absorber like other trace gases, and no treatment of elastic scattering is considered. To determine the magnitude of possible biases resulting from these differing assumptions a comparison exercise was established. As with the OMNO2A retrieval, a composite set of solar irradiance reference spectra derived from OMI irradiance data (OML1BIRR, v 3.0, Van den Oord et al., 2006) taken during 2005 was used in this initial test. These were used to retrieve total NO_2 SCDs in cloud-free regions (i.e. pixel cloud fraction < 25 %) over the whole globe during June 2005, using the retrieval parameters shown in Table 1, as care was taken to ensure that the cross-sections, interpolation method and retrieval settings employed were a close approximation to those used in the OMNO2A retrieval. The resulting SCDs and uncertainties were then compared with those retrieved by OMNO2A, as shown in Fig. 4.

The results show an almost constant negative bias between the QDOAS-based retrieval and OMNO2A over all regions for both the SCD and the uncertainty (average SCD bias $\sim -1.0 \times 10^{15}$ molec cm^{-2}). There appear to be no geospatial features in either plot other than a slightly stronger bias over mountainous regions, potentially due to possible retrieval sensitivity to surface albedo. The lack of spatial features suggests that this bias is the result of some flaw in the retrieval algorithm, rather than any unforeseen geophysical process.

Additionally, the bias also exhibits a strong across-track variation, as shown in Fig. 5. The reason for this effect is currently unknown. One possible cause could be how QDOAS treats spectral pixels flagged for removal due to random telegraph signals or dark current behaviour (Van den Oord et al., 2006); the number of pixels that need to be removed from the DOAS fit for this reason varies between across-track pixels, which may add to the bias caused by the retrieval algorithm differences.

As a result, comparisons between the retrievals covered in this paper with existing retrievals were conducted using only ground pixels in which the QDOAS-based retrieval using solar reference spectra produced total SCDs that were within 5 % of the total SCDs produced by OMNO2A. It was assumed that ESrs-DOAS retrievals of NO_2

AMTD
7, 6699–6742, 2014

over such pixels using the QDOAS software would be representative of what would be retrieved if the ESrs-DOAS fits were performed using the OMNO2A software, as they would be relatively free from this bias.

3.3 DOAS retrieval using earthshine reference spectra

For the first phase of this study earthshine radiance spectra recorded during June 2005 were considered. Daily earthshine radiance data from a Pacific reference sector (125–180° W, 60° S–60° N) over this month were binned into a set of 60 reference spectra for each OMI across-track pixel. To account for the latitudinal gradient in stratospheric NO_2 the spectra were also binned into 1° latitude bins, such that DOAS retrievals of earthshine spectra observed over the rest of the planet made use of the reference spectra obtained from the closest latitude bin.

Using a latitudinal reference sector also resolves potential biases resulting from changes in SZA between the reference and observed region. Observations made with high SZAs will be more sensitive to the stratosphere due to an increase the in mean scattering height (Hendrick et al., 2004; Preston et al., 1997), which may result in unforseen stratospheric contamination in the SCDs retrieved with this method. However, as OMI follows a sun-synchronous orbit, the ground pixel SZA is dependent on latitude and season. As a result, using a daily, latitudinally binned reference spectrum means that the difference in SZA between the reference and observed region will be negligible, so this effect will be negated.

It was determined that only spectra that were measured over largely cloud-free scenes (i.e. cloud fraction < 25 %) would be binned to this dataset. Scattering from clouds would lead to inhomogeneous illumination of the OMI entrance slit, which in turn leads to a change in the position and shape of the instrument slit function. The change in the slit function then results in an observed shift in the wavelength mapping of the Fraunhofer lines on the detector (Voors et al., 2006). As the DOAS fit depends on good wavelength calibration, cloudy pixels would need to be avoided to obtain the

AMTD
7, 6699–6742, 2014

best possible result in this work. As well as this, using cloudy scenes would otherwise introduce a cloud height dependence on the inherent stratospheric NO_2 retrieved.

As shown in Fig. 6a and b the ESrs-DOAS retrieval shows good correlation with tropospheric SCDs retrieved by DOMINO, particularly showing good spatial similarity with megacities and regions with known anthropogenic activity (e.g. mining), as well as possible biomass burning over central Africa. However, the retrieval produces significant, broad negative biases over remote regions such as Tibet, particularly at higher northern latitudes over land. This is potentially due to undersampling of reference spectra in the Pacific reference sector resulting from excessive cloud cover at those latitudes, which would result in a degradation in the quality of the DOAS fit and an underestimation of the local stratospheric field; both factors would result in lower SCDs retrieved. As well as this, Fig. 6d shows that the stratospheric NO_2 field varies considerably with longitude at the latitudes where this bias appears. This variation is especially pronounced in the Pacific reference sector, which has higher stratospheric SCDs compared with other longitudes. The increased NO_2 absorption present in the reference sector would therefore lead to lower tropospheric SCDs retrieved over other areas.

One particularly significant positive bias appears over the region (70° W–160° E, 16–22° S) and the Southern Ocean, in which the retrieval overestimates the magnitude and spatial spread of the tropospheric NO_2 band that is detected in the DOMINO retrieval (Fig. 6b). According to the assimilated stratospheric NO_2 available from DOMINO (Fig. 6d) these regions had considerable longitudinal variation in stratospheric fields compared with the Pacific reference sector, which would result in the Pacific reference sector being an underestimate of the local stratospheric field. Both of these cases show the need to accurately estimate the stratospheric NO_2 field and to have enough cloud-free measurements in the reference sector in order for this type of retrieval to be successful.

It was found over the course of this study that the earthshine reference retrieval produces anomalously high root mean square error (RMS) values over regions such as the Sahara and Namibian deserts, as well as the Atlantic and Pacific oceans. The fine

AMTD
7, 6699–6742, 2014

structure present in the residual spectra retrieved over these regions suggested that another absorber unaccounted for by the DOAS fit may be active over these regions. The spatial range of these anomalous regions appear to be similar to those encountered by Richter et al. (2011) when investigating improvements to the GOME-2 NO_2 retrieval. It was discovered through adding a liquid water and sand (empirically measured using GOME-2 spectra) absorption cross section to the DOAS fit that the RMS and NO_2 SCD uncertainty decreased over these regions. As shown in Fig. 2 these absorption cross sections are sufficiently different from purely polynomial functions, and so cannot be accounted for by the polynomial term used in the fit. Therefore, the polynomial used in the earthshine DOAS fits was also simplified from a 5th to 3rd order to prevent these features from interfering with the fit.

To illustrate this effect tropospheric NO_2 SCDs were retrieved from OMI spectra recorded over the Sahara desert during June 2005 using an earthshine reference with these added cross sections. The RMS of these DOAS fits were compared with those resulting from DOAS fits with an earthshine reference, but using only the same cross sections that are used in OMNO2A (see Table 1). As shown in Fig. 7, the addition of the sand and liquid water cross-sections resulted in a reduction in RMS over the whole region.

The resulting plots for retrieved liquid water and sand fit coefficients over the same month are shown in Fig. 8. These plots show a remarkable spatial similarity with the GOME-2 retrieval results, which suggests that accounting for this contamination will need to be addressed in future instrument and retrieval designs. Despite this similarity, there are also anomalously high water and sand fit coefficients retrieved over extreme northern latitudes. As with the negative NO_2 bias at these latitudes this could potentially be the result of artefacts introduced by having undersampled reference spectra at the corresponding Pacific reference sectors.

AMTD
7, 6699–6742, 2014

3.4 Urban transect comparison

In order to determine the sensitivity of this retrieval to the relative difference in NO_2 between urban and rural areas a comparison exercise was undertaken between the earthshine reference retrieval, OMNO2, and DOMINO. As shown in Fig. 9, the mean tropospheric NO_2 SCDs retrieved during June 2005 are selected over a latitudinal transect across China, from Hong Kong to Inner Mongolia (20–50° N, 114° E). The average tropospheric SCD retrieved using an earthshine reference spectrum during June 2005 is compared with that retrieved by the DOMINO and OMNO2 algorithms.

The earthshine reference retrieval demonstrates sensitivity to NO_2 enhancement over urban areas, as the latitudinal variation is very similar to that exhibited by the DOMINO and OMNO2 transects. Over the Pearl River Delta (23° N) the SCDs retrieved by all three algorithms appear to be nearly identical, while enhancement over other urban areas is also detected by the earthshine retrieval and shows good agreement with the other algorithms. However, further along the transect there is a consistent negative offset associated with the earthshine retrieval, particularly over Inner Mongolia (45–50° N), though this bias appears to be largely within the mean uncertainty of the DOAS fit as reported by QDOAS.

One significant uncertainty in this analysis is that the temperature sensitivity of the NO_2 cross-section is not accounted for in the earthshine reference retrievals. As with other DOAS retrievals of NO_2 a cross-section at a single, stratospheric temperature is used (220 K) to retrieve the SCD, while the influence of the temperature profile on the NO_2 absorption is accounted for in the AMF computation, through weighting the AMF with an empirically derived correction factor for each atmospheric layer considered (e.g. Bucsela et al., 2013; Boersma et al., 2004). Neglecting this effect can result in underestimating the NO_2 in polluted areas by up to to 20 %, as the boundary-layer NO_2 is much warmer than the stratospheric cross-section used in the DOAS fit. Both the DOMINO and OMNO2 tropospheric SCDs have been derived from VCDs which in

AMTD
7, 6699–6742, 2014

turn were calculated to account for this effect, which would potentially explain the bias between these datasets and the earthshine reference retrieval.

As well as this, the residual bias could also be exacerbated by longitudinal differences in stratospheric NO_2 over the Pacific reference sector and China, which could not be accounted for when collecting reference spectra. Despite the presence of such biases, the sensitivity to tropospheric NO_2 variability demonstrates that this technique could be used to retrieve spatially resolved tropospheric NO_2 over urban areas.

3.5 Retrieval using local reference sector over South Africa

A significant issue when using reference spectra from a single location is that differences in the local tropospheric and stratospheric NO_2 field can lead to substantial biases in estimating tropospheric NO_2 over other longitudes. One possible solution is to use reference spectra from an area closer to the region of interest in order to provide a better representation of the local stratospheric field. Such regions may also be comparatively cloud-free, which would lead to better sampling of reference spectra. To determine the validity of this technique a comparison exercise is set up over a region covering South Africa. This region is particularly interesting as South Africa has the largest industrialised economy in Africa, with major cities and anthropogenic activities such as mining and agriculture primarily centred around Bushveld and Highveld. Because of this, these regions are considered to be air quality hotspots, and have been the subject of several studies to determine the impact emissions from these regions have on ambient air quality (e.g. Josipovic et al., 2010; Lourens et al., 2011; Venter et al., 2012). The region is an ideal candidate for determining the impact of this technique on retrieval accuracy, as it is distant from other NO_2 sources which allows for both point sources and pollution transport to be clearly visible.

For this study earthshine radiance spectra measured during June 2005 are analysed over the region (20–40° S, 50° W–80° E). Here, the earthshine reference spectra are instead collected from the South Atlantic (20–40° S, 0° W–30° E) for use in the DOAS fit. The reference region was chosen as it was close to the region of interest, while still

AMTD
7, 6699–6742, 2014

being distant enough to avoid tropospheric contamination from pollution transport. Figure 10 shows a comparison between tropospheric SCDs retrieved using this reference sector, the Pacific reference sector and the DOMINO product. Using a nearby reference sector improves correlation with the DOMINO results, while removing the longitudinal bias present beyond ~ 23° S.

3.6 Improvement in striping reduction

In order to determine the impact the ESrs-DOAS technique has on removing across-track striping all retrievals in a single OMI swath from a region in the Pacific deemed to be distant from tropospheric pollution sources and the reference sector (30° S–5° N, 90–130° W) are analysed. All SCDs retrieved using the multiple earthshine reference algorithms over this region for each across-track pixel are averaged to form a single dataset. The mean is then subtracted in order to determine the across-track variability between pixels. This is then repeated with corresponding data from DOMINO and OMNO2.

As shown in Fig. 11, the reduction in across-track variability when using multiple earthshine reference spectra is greater than the existing destriping algorithms used by OMNO2 and DOMINO, suggesting that this technique could be used to account for biases resulting from instrument design without post hoc filtering. The technique also appears to account for the bias introduced by light path enhancement due to viewing geometry at the edges of the swath.

3.7 SCD uncertainty estimation

In order to determine the effect of random noise has on the retrievals a statistical approach similar to those conducted by Richter et al. (2011) and Valks et al. (2011). An area over the Pacific that was assumed to be relatively unpolluted is chosen (100–120° W, 10° N–10° S) and the tropospheric NO_2 retrieved during June 2005 is analysed. It is assumed that the stratospheric NO_2 over this region and timescale is both

AMTD
7, 6699–6742, 2014

temporally and spatially invariant, so the the spread in these measurements would primarily originate from the inherent accuracy of the retrieval. To measure this spread the SCDs retrieved over this region using the earthshine reference, and OMNO2A algorithms are scaled with a geometric AMF, in order to account for variability introduced by the changing SZA and viewing geometry over this area and period. These SCDs are then binned to $2^{\circ} \times 2^{\circ}$ boxes, from which the deviation from the mean over each SCD is recorded. These deviations are subsequently binned to a histogram to determine the spread of the measurements. It was found that these histograms could be modelled as Gaussian functions, so the retrieval error can represented by the standard deviation, σ, of the distribution.

The OMNO2A SCDs has a σ of 1.1×10^{15} molec cm^{-2}. This value is similar to that derived from the total SCDs retrieved by emulating the OMNO2A algorithm using QDOAS. The earthshine retrieval, however, produces a σ of 8.0×10^{14} molec cm^{-2}, which corresponds to a $\sim 27\,\%$ reduction in random error using this retrieval. This is most likely due to the reduction in the across-track striping, as these features still remain in the OMNO2A SCDs. Figure 12 shows the distribution and the fitted Gaussian function for the earthshine reference retrievals.

This analysis was carried out over all pixels retrieved over the specified region between 2005–2008, with the resulting time series shown in Fig. 13. Both the earthshine and solar retrieval uncertainties appear to be subject to an annual cycle, with peak values occurring around June. From regression analysis it was determined that the best fit of the data was achieved when accounting for this cycle (up to the 2nd harmonic in a Fourier series) in addition to a linear trend. This cycle could potentially be related to the periodicity of the insolation observed over the area during the year, though the physical meaning behind the 2nd harmonic is currently unknown. This model also does not fit the solar retrieval uncertainty trends as well as the earthshine retrieval, suggesting that that DOAS fits using a solar reference are subject to some other factor, such as changes in the solar irradiance reference spectrum. Such changes over time would not be accounted for, as both the OMNO2A and QDOAS solar retrievals only use the

AMTD
7, 6699–6742, 2014

composite irradiance reference spectra measured in 2005 previously described in this work.

In addition to the annual cycle there appears to be a statistically significant positive trend for all three time series, which may be the result of instrument degradation during this time period. The trend for the earthshine retrieval uncertainty (1.5×10^{13} molec cm^{-2} month^{-1}) is much lower than that of the solar retrieval uncertainty, (5.8×10^{13} molec cm^{-2} month^{-1}), potentially demonstrating this technique's resilience to degradation.

4 Summary and conclusions

This work has shown that earthshine reference spectra from the remote Pacific in a satellite NO_2 DOAS fit can be used to retrieve tropospheric NO_2 SCDs over polluted regions with minimal need for model assimilation or spatial filtering. Figure 3 shows that the NO_2 SCD derived from using an earthshine reference is (within retrieval error) equivalent to the difference between the total NO_2 SCD retrieved over the reference region and the region of interest. The NO_2 profile can be partitioned into clearly defined tropospheric and stratospheric components, which makes this technique ideal for tropospheric NO_2 retrieval provided that the stratospheric component is the same over both the reference region and the region of interest. As shown in Fig. 6d the stratospheric field is not longitudinally homogeneous, particularly at extreme latitudes. These variations can result in significant biases in tropospheric NO_2 retrieved with this method compared with the model-assimilated DOMINO SCDs. One possible method in resolving these biases would be to use reference spectra from regions closer to the observation, though this limits the efficacy of this retrieval technique to coastal regions or other areas close to regions where tropospheric contamination could be minimised (e.g. deserts).

Despite the magnitude of the biases compared with DOMINO, the earthshine reference retrieval appears to give spatially consistent results. As shown in the urban

AMTD
7, 6699–6742, 2014

transect comparison (Fig. 9) the retrieval shows sensitivity to the tropospheric NO_2 enhancement owing to anthropogenic activity, as the average transect for all three retrieval algorithms show good correlation. The bias in the earthshine reference retrieval appears as a near-consistent offset, potentially due to the retrieval not accounting for the impact the temperature gradient has on NO_2 absorption. However, the bias also appears to increase over the comparatively unpolluted Inner Mongolia region, which suggests that residual biases owing to the longitudinal variation in stratospheric NO_2 or temperature have a significant impact over remote unpolluted regions.

Using the uncertainty derivation technique defined by Valks et al. (2011) it was found that the earthshine reference resulted in ~ 27 % reduction in retrieval uncertainty. Time series analysis shows that the retrieval uncertainty owing to instrument degradation may be much less when using an earthshine reference. The retrieval technique also largely resolves the biases resulting from across-track striping with a minimal need for a posteriori corrections.

However, the benefits using the ESrs-DOAS technique have only been defined for cloud-free scenes. In cloudier scenes the photons will be scattered more, which will result in greater retrieval uncertainty. In the case of using earthshine reference spectra this issue is exacerbated by the influence cloud top height may have on the assumed stratospheric component. The wavelength shifts caused by cloud cover (Voors et al., 2006) are also an issue when selecting earthshine spectra, and need to be empirically corrected before binning. Future satellite instruments that would utilise this technique will therefore need to have a robust wavelength calibration. Despite the issues in wavelength calibration, there is some potential in using the cloud layer to determine the free tropospheric amount of NO_2 based on the established cloud slicing technique used in some cases to retrieve tropospheric O_3 and NO_2 (Choi et al., 2014; Ziemke et al., 2001).

It was noted that the retrieval shows sensitivity to absorption from sand and liquid water, as shown by the spatial distributions retrieved in Fig. 8 and the reduction in RMS in Fig. 7 when these absorbers were included in the fit. The spatial similarity

AMTD
7, 6699–6742, 2014

of the features retrieved with those found by Richter et al. (2011) suggest that these features are the result of real absorption rather than an instrument specific defect, and should be included in future retrieval algorithms. Previously Merlaud et al. (2012) discussed potential correlations between O_2-O_2 absorption and sand, as both cross-sections have distinct peaks at ∼ 477 nm. Currently the fitting window employed by OMNO2A does not extend to this wavelength, as absorption from O_2-O_2 has no impact on retrieval accuracy (Boersma et al., 2007). This algorithm could potentially utilise a larger fitting window to identify absorption from both species and to retrieve aerosol information based on their absorption.

This work has only covered derivation of the tropospheric SCD, while an operational version of this technique will need to consider an appropriate AMF derivation. In the DOMINO algorithm Boersma et al. (2011) the tropospheric AMF is calculated after the stratospheric component has been subtracted from the total VCD. In this scenario, however, only a differential SCD has been measured, where the stratospheric column has been implicitly defined, rather than explicitly measured. A similar scenario is found in aircraft DOAS measurements (e.g. Popp et al., 2012), in which the reference spectrum is also taken from measurements over a region that is assumed to be unpolluted. The tropospheric VCD calculation therefore has to estimate the VCD of the reference region, such as using a reference climatology. However, in regions such as the remote Pacific the tropospheric contribution is likely to be negligible, so such a correction would only be required if a reference region close to the observation is chosen.

The technique detailed in this work could potentially be used to retrieve tropospheric NO_2 over urban regions using a smaller and simpler spectrometer design than current instruments, as there would be no need for a solar reference measurement. The reduced cost would enable such a design to be employed as part of a constellation of instruments to provide tropospheric VCDs at a much greater temporal resolution than currently possible with single instruments. The reduced across-track variability (as shown in Fig. 11) indicates that no comparison with adjacent orbits is required to remove across-track stripes, which potentially reduces the required time between

AMTD
7, 6699–6742, 2014

spectral measurement and final data publication. The observed reduction in uncertainty due to striping and instrument degradation also shows that the technique is inherently self-correcting for such defects. This could in turn would allow long mission lifetimes resulting in the creation of reliable long-term datasets, such as the decade-long dataset provided by SCIAMACHY measurements (e.g. Huang et al., 2013).

Acknowledgements. This research was financially supported as part of a PhD studentship provided by the UK Centre for Earth Observation and Instrumentation (CEOI). We acknowledge the use of OMI L1B and L2 data made available from the NASA MIRADOR (http://disc.sci.gsfc.nasa.gov/Aura/data-holdings/OMI) and KNMI TEMIS (http://www.temis.nl) services. The QDOAS software package and continued support were kindly provided by M. van Roozendael, C. Fayt, and the DOAS group of BIRA/IASB. We are grateful for the assistance KNMI have provided us in understanding the OMNO2A retrieval algorithm, particularly F. Boersma, J. van Geffen, M. Sneep, and P. Veefkind. We are also grateful to J. Remedios (University of Leicester) for his helpful comments.

References

Acarreta, J. R., De Haan, J. F., and Stammes, P.: Cloud pressure retrieval using the O_2-O_2 absorption band at 477 nm, J. Geophys. Res.-Atmos., 109, D05204, doi:10.1029/2003JD003915, 2004. 6705

Boersma, K. F., Eskes, H. J., and Brinksma, E. J.: Error analysis for tropospheric NO_2 retrieval from space, J. Geophys. Res.-Atmos., 109, D04331, doi:10.1029/2003JD003962, 2004. 6701, 6703, 6704, 6714

Boersma, K. F., Eskes, H. J., Veefkind, J. P., Brinksma, E. J., van der A, R. J., Sneep, M., van den Oord, G. H. J., Levelt, P. F., Stammes, P., Gleason, J. F., and Bucsela, E. J.: Near-real time retrieval of tropospheric NO_2 from OMI, Atmos. Chem. Phys., 7, 2103–2118, doi:10.5194/acp-7-2103-2007, 2007. 6701, 6705, 6706, 6707, 6720, 6729

Boersma, K. F., Eskes, H. J., Dirksen, R. J., van der A, R. J., Veefkind, J. P., Stammes, P., Huijnen, V., Kleipool, Q. L., Sneep, M., Claas, J., Leitão, J., Richter, A., Zhou, Y., and Brunner, D.: An improved tropospheric NO_2 column retrieval algorithm for the Ozone Monitoring

AMTD
7, 6699–6742, 2014

Instrument, Atmos. Meas. Tech., 4, 1905–1928, doi:10.5194/amt-4-1905-2011, 2011. 6706, 6720

Bogumil, K., Orphal, J., Voigt, S., Bovensmann, H., Fleischmann, O., Hartmann, M., Homann, T., Spietz, P., Vogel, A., and Burrows, J.: Reference spectra of atmospheric trace gases measured with the SCIAMACHY PFM satellite spectrometer, Proc. 1st Europ. Sympos. Atmos. Meas. from Space (ESAMS-99), 2, 443–447, 1999. 6729

Braak, R.: Row Anomaly Flagging Rules Lookup Table, KNMI Technical Document, TN-OMIE-KNMI-950, 2010. 6708

Bucsela, E., Celarier, E., Wenig, M., Gleason, J., Veefkind, J., Boersma, K., and Brinksma, E.: Algorithm for NO_2 vertical column retrieval from the Ozone Monitoring Instrument, IEEE T. Geosci. Remote, 44, 1245–1258, doi:10.1109/TGRS.2005.863715, 2006. 6701, 6702, 6704, 6705, 6708

Bucsela, E. J., Krotkov, N. A., Celarier, E. A., Lamsal, L. N., Swartz, W. H., Bhartia, P. K., Boersma, K. F., Veefkind, J. P., Gleason, J. F., and Pickering, K. E.: A new stratospheric and tropospheric NO_2 retrieval algorithm for nadir-viewing satellite instruments: applications to OMI, Atmos. Meas. Tech., 6, 2607–2626, doi:10.5194/amt-6-2607-2013, 2013. 6705, 6714

Burrows, J. P., Weber, M., Buchwitz, M., Rozanov, V., Ladstätter-Weißenmayer, A., Richter, A., Debeek, R., Hoogen, R., Bramstedt, K., Eichmann, K.-U., Eisinger, M., and Perner, D.: The Global Ozone Monitoring Experiment (GOME): mission concept and first scientific results, J. Atmos. Sci., 56, 151–175, doi:10.1175/1520-0469(1999)056<0151:TGOMEG>2.0.CO;2, 1999. 6701

Celarier, E. A., Brinksma, E. J., Gleason, J. F., Veefkind, J. P., Cede, A., Herman, J. R., Ionov, D., Goutail, F., Pommereau, J.-P., Lambert, J.-C., van Roozendael, M., Pinardi, G., Wittrock, F., Schönhardt, A., Richter, A., Ibrahim, O. W., Wagner, T., Bojkov, B., Mount, G., Spinei, E., Chen, C. M., Pongetti, T. J., Sander, S. P., Bucsela, E. J., Wenig, M. O., Swart, D. P. J., Volten, H., Kroon, M., and Levelt, P. F.: Validation of Ozone Monitoring Instrument nitrogen dioxide columns, J. Geophys. Res.-Atmos., 113, D15S15, doi:10.1029/2007JD008908, 2008. 6706

Celarier, E. A., Gleason, J. F., Bucsela, E. J., Boersma, K. F., Brinksma, E., Veefkind, J. P., and Levelt, P.: OMNO2 README file, technical report, NASA Goddard Space Flight Cent., Greenbelt, Md, available at: http://disc.sci.gsfc.nasa.gov/Aura/data-holdings/OMI/documents/v003/OMNO2_readme_v003.pdf (last access: 5 March 2014), 2013. 6705

AMTD
7, 6699–6742, 2014

Chameides, W. L., Fehsenfeld, F., Rodgers, M. O., Cardelino, C., Martinez, J., Parrish, D., Lonneman, W., Lawson, D. R., Rasmussen, R. A., Zimmerman, P., Greenberg, J., Mlddleton, P., and Wang, T.: Ozone precursor relationships in the ambient atmosphere, J. Geophys. Res.-Atmos., 97, 6037–6055, doi:10.1029/91JD03014, 1992. 6701

Chance, K. V. and Spurr, R. J. D.: Ring effect studies: Rayleigh scattering, including molecular parameters for rotational Raman scattering, and the Fraunhofer spectrum, Appl. Optics, 36, 5224–5230, doi:10.1364/AO.36.005224, 1997. 6702, 6703

Choi, S., Joiner, J., Choi, Y., Duncan, B. N., and Bucsela, E.: Global free tropospheric NO_2 abundances derived using a cloud slicing technique applied to satellite observations from the Aura Ozone Monitoring Instrument (OMI), Atmos. Chem. Phys. Discuss., 14, 1559–1615, doi:10.5194/acpd-14-1559-2014, 2014. 6719

De Smedt, I., Müller, J.-F., Stavrakou, T., van der A, R., Eskes, H., and Van Roozendael, M.: Twelve years of global observations of formaldehyde in the troposphere using GOME and SCIAMACHY sensors, Atmos. Chem. Phys., 8, 4947–4963, doi:10.5194/acp-8-4947-2008, 2008. 6702

Dirksen, R. J., Boersma, K. F., Eskes, H. J., Ionov, D. V., Bucsela, E. J., Levelt, P. F., and Kelder, H. M.: Evaluation of stratospheric NO_2 retrieved from the Ozone Monitoring Instrument: intercomparison, diurnal cycle, and trending, J. Geophys. Res.-Atmos., 116, D08305, doi:10.1029/2010JD014943, 2011. 6706

Dobber, M., Dirksen, R., Voors, R., Mount, G. H., and Levelt, P.: Ground-based zenith sky abundances and in situ gas cross sections for ozone and nitrogen dioxide with the Earth Observing System Aura Ozone Monitoring Instrument, Appl. Optics, 44, 2846–2856, doi:10.1364/AO.44.002846, 2005. 6708

Dobber, M., Kleipool, Q., Dirksen, R., Levelt, P., Jaross, G., Taylor, S., Kelly, T., Flynn, L., Leppelmeier, G., and Rozemeijer, N.: Validation of Ozone Monitoring Instrument level 1b data products, J. Geophys. Res.-Atmos., 113, D15S06, doi:10.1029/2007JD008665, 2008a. 6708

Dobber, M., Voors, R., Dirksen, R., Kleipool, Q., and Levelt, P.: The high-resolution solar reference spectrum between 250 and 550 nm and its application to measurements with the Ozone Monitoring Instrument, Sol. Phys., 249, 281–291, doi:10.1007/s11207-008-9187-7, 2008b. 6708

Fayt, C., De Smedt, I., Letocart, V., Merlaud, A., Pinardi, G., and Van Roozendael, M.: QDOAS Software user manual, BIRA-IASB, available at: http://uv-vis.aeronomie.be/software/QDOAS/index.php (last access: 3 February 2014), 2013. 6706, 6738

AMTD
7, 6699–6742, 2014

Hains, J. C., Boersma, K. F., Kroon, M., Dirksen, R. J., Cohen, R. C., Perring, A. E., Bucsela, E., Volten, H., Swart, D. P. J., Richter, A., Wittrock, F., Schoenhardt, A., Wagner, T., Ibrahim, O. W., van Roozendael, M., Pinardi, G., Gleason, J. F., Veefkind, J. P., and Levelt, P.: Testing and improving OMI DOMINO tropospheric NO_2 using observations from the DANDELIONS and INTEX-B validation campaigns, J. Geophys. Res.-Atmos., 115, D05301, doi:10.1029/2009JD012399, 2010. 6701

Hendrick, F., Barret, B., Van Roozendael, M., Boesch, H., Butz, A., De Mazière, M., Goutail, F., Hermans, C., Lambert, J.-C., Pfeilsticker, K., and Pommereau, J.-P.: Retrieval of nitrogen dioxide stratospheric profiles from ground-based zenith-sky UV-visible observations: validation of the technique through correlative comparisons, Atmos. Chem. Phys., 4, 2091–2106, doi:10.5194/acp-4-2091-2004, 2004. 6711

Hewson, W., Bösch, H., Barkley, M. P., and De Smedt, I.: Characterisation of GOME-2 formaldehyde retrieval sensitivity, Atmos. Meas. Tech., 6, 371–386, doi:10.5194/amt-6-371-2013, 2013. 6707

Huang, J., Zhou, C., Lee, X., Bao, Y., Zhao, X., Fung, J., Richter, A., Liu, X., and Zheng, Y.: The effects of rapid urbanization on the levels in tropospheric nitrogen dioxide and ozone over East China, Atmos. Environ., 77, 558–567, doi:10.1016/j.atmosenv.2013.05.030, 2013. 6721

Huijnen, V., Eskes, H. J., Poupkou, A., Elbern, H., Boersma, K. F., Foret, G., Sofiev, M., Valdebenito, A., Flemming, J., Stein, O., Gross, A., Robertson, L., D'Isidoro, M., Kioutsioukis, I., Friese, E., Amstrup, B., Bergstrom, R., Strunk, A., Vira, J., Zyryanov, D., Maurizi, A., Melas, D., Peuch, V.-H., and Zerefos, C.: Comparison of OMI NO_2 tropospheric columns with an ensemble of global and European regional air quality models, Atmos. Chem. Phys., 10, 3273–3296, doi:10.5194/acp-10-3273-2010, 2010. 6701

Josipovic, M., Annegarn, H., Kneen, M., Pienaar, J., and Piketh, S.: Concentrations, distributions and critical level exceedance assessment of SO_2, NO_2 and O_3 in South Africa, Environ. Monit. Assess., 171, 181–196, doi:10.1007/s10661-009-1270-5, doi:10.1007/s10661-009-1270-5, 2010. 6715

Kleipool, Q. L., Dobber, M. R., de Haan, J. F., and Levelt, P. F.: Earth surface reflectance climatology from 3 years of OMI data, J. Geophys. Res.-Atmos., 113, D18308, doi:10.1029/2008JD010290, 2008. 6705

Konovalov, I. B., Beekmann, M., Richter, A., Burrows, J. P., and Hilboll, A.: Multi-annual changes of NO_x emissions in megacity regions: nonlinear trend analysis of satellite mea-

AMTD
7, 6699–6742, 2014

surement based estimates, Atmos. Chem. Phys., 10, 8481–8498, doi:10.5194/acp-10-8481-2010, 2010. 6701
Levelt, P., Van den Oord, G. H. J., Dobber, M., Malkki, A., Visser, H., de Vries, J., Stammes, P., Lundell, J., and Saari, H.: The Ozone Monitoring Instrument, IEEE T. Geosci. Remote, 44, 1093–1101, doi:10.1109/TGRS.2006.872333, 2006. 6701, 6704
Lourens, A., Beukes, J., van Zyl, P., Fourie, G., Burger, J., Pienaar, J., Read, C., and Jordaan, J.: Spatial and temporal assessment of gaseous pollutants in the Highveld of South Africa, S. Afr. J. Sci., 107, 1–8, doi:10.4102/sajs.v107i1/2.269, 2011. 6715
Merlaud, A., Van Roozendael, M., van Gent, J., Fayt, C., Maes, J., Toledo-Fuentes, X., Ronveaux, O., and De Mazière, M.: DOAS measurements of NO_2 from an ultralight aircraft during the Earth Challenge expedition, Atmos. Meas. Tech., 5, 2057–2068, doi:10.5194/amt-5-2057-2012, 2012. 6720
Monks, P. and Beirle, S.: Applications of satellite observations of tropospheric composition, in: The Remote Sensing of Tropospheric Composition from Space, edited by: Burrows, J. P., Borrell, P., and Platt, U., Physics of Earth and Space Environments, Springer, Berlin, Heidelberg, 365–449, doi:10.1007/978-3-642-14791-3_8, 2011. 6701
Platt, U. and Stutz, J.: Differential Optical Absorption Spectroscopy (DOAS), Principle and Applications, Springer Verlag, 2006. 6702
Pope, R. M. and Fry, E. S.: Absorption spectrum (380–700 nm) of pure water. II. Integrating cavity measurements, Appl. Optics, 36, 8710–8723, doi:10.1364/AO.36.008710, 1997. 6729
Popp, C., Brunner, D., Damm, A., Van Roozendael, M., Fayt, C., and Buchmann, B.: High-resolution NO_2 remote sensing from the Airborne Prism EXperiment (APEX) imaging spectrometer, Atmos. Meas. Tech., 5, 2211–2225, doi:10.5194/amt-5-2211-2012, 2012. 6707, 6720
Preston, K. E., Jones, R. L., and Roscoe, H. K.: Retrieval of NO_2 vertical profiles from ground-based UV-visible measurements: method and validation, J. Geophys. Res.-Atmos., 102, 19089–19097, doi:10.1029/97JD00603, 1997. 6711
Richter, A. and Burrows, J. P.: Tropospheric NO_2 from GOME measurements, Adv. Space Res., 29, 1673–1683, doi:10.1016/S0273-1177(02)00100-X, 2002. 6702
Richter, A., Eyring, V., Burrows, J. P., Bovensmann, H., Lauer, A., Sierk, B., and Crutzen, P. J.: Satellite measurements of NO_2 from international shipping emissions, Geophys. Res. Lett., 31, L23110, doi:10.1029/2004GL020822, 2004. 6701

AMTD
7, 6699–6742, 2014

Richter, A., Begoin, M., Hilboll, A., and Burrows, J. P.: An improved NO_2 retrieval for the GOME-2 satellite instrument, Atmos. Meas. Tech., 4, 1147–1159, doi:10.5194/amt-4-1147-2011, 2011. 6713, 6716, 6720, 6729

Rothman, L., Jacquemart, D., Barbe, A., Benner, D. C., Birk, M., Brown, L., Carleer, M., Chackerian Jr., C., Chance, K., Coudert, L., Dana, V., Devi, V., Flaud, J.-M., Gamache, R., Goldman, A., Hartmann, J.-M., Jucks, K., Maki, A., Mandin, J.-Y., Massie, S., Orphal, J., Perrin, A., Rinsland, C., Smith, M., Tennyson, J., Tolchenov, R., Toth, R., Auwera, J. V., Varanasi, P., and Wagner, G.: The HITRAN 2004 molecular spectroscopic database, J. Quant. Spectrosc. Ra., 96, 139–204, doi:10.1016/j.jqsrt.2004.10.008, 2005. 6729

Rothman, L., Gordon, I., Barbe, A., Benner, D., Bernath, P., Birk, M., Boudon, V., Brown, L., Campargue, A., Champion, J.-P., Chance, K., Coudert, L., Dana, V., Devi, V., Fally, S., Flaud, J.-M., Gamache, R., Goldman, A., Jacquemart, D., Kleiner, I., Lacome, N., Lafferty, W., Mandin, J.-Y., Massie, S., Mikhailenko, S., Miller, C., Moazzen-Ahmadi, N., Naumenko, O., Nikitin, A., Orphal, J., Perevalov, V., Perrin, A., Predoi-Cross, A., Rinsland, C., Rotger, M., Šimečková, M., Smith, M., Sung, K., Tashkun, S., Tennyson, J., Toth, R., Vandaele, A., and Auwera, J. V.: The HITRAN 2008 molecular spectroscopic database, J. Quant. Spectrosc. Ra., 110, 533–572, doi:10.1016/j.jqsrt.2009.02.013, 2009. 6729

Rozanov, A., Rozanov, V., Buchwitz, M., Kokhanovsky, A., and Burrows, J.: SCIATRAN 2.0 – a new radiative transfer model for geophysical applications in the 175–2400 nm spectral region, Adv. Space Res., 36, 1015–1019, doi:10.1016/j.asr.2005.03.012, 2005. 6707

Russell, A. R., Perring, A. E., Valin, L. C., Bucsela, E. J., Browne, E. C., Wooldridge, P. J., and Cohen, R. C.: A high spatial resolution retrieval of NO_2 column densities from OMI: method and evaluation, Atmos. Chem. Phys., 11, 8543–8554, doi:10.5194/acp-11-8543-2011, 2011. 6706

Schönhardt, A., Richter, A., Wittrock, F., Kirk, H., Oetjen, H., Roscoe, H. K., and Burrows, J. P.: Observations of iodine monoxide columns from satellite, Atmos. Chem. Phys., 8, 637–653, doi:10.5194/acp-8-637-2008, 2008. 6702

Sierk, B., Richter, A., Rozanov, A., Savigny, C., Schmoltner, A., Buchwitz, M., Bovensmann, H., and Burrows, J.: Retrieval and monitoring of atmospheric trace gas concentrations in nadir and limb geometry using the Space-Borne Sciamachy Instrument, Environ. Monit. Assess., 120, 65–77, doi:10.1007/s10661-005-9049-9, 2006. 6702

AMTD
7, 6699–6742, 2014

Valin, L. C., Russell, A. R., Bucsela, E. J., Veefkind, J. P., and Cohen, R. C.: Observation of slant column NO_2 using the super-zoom mode of AURA-OMI, Atmos. Meas. Tech., 4, 1929–1935, doi:10.5194/amt-4-1929-2011, 2011. 6704

Valks, P., Pinardi, G., Richter, A., Lambert, J.-C., Hao, N., Loyola, D., Van Roozendael, M., and Emmadi, S.: Operational total and tropospheric NO_2 column retrieval for GOME-2, Atmos. Meas. Tech., 4, 1491–1514, doi:10.5194/amt-4-1491-2011, 2011. 6716, 6719

Van den Oord, G. H. J., Rozemeijer, N., Schenkelaars, V., Levelt, P., Dobber, M., Voors, R., Claas, J., de Vries, J., ter Linden, M., De Haan, C., and Van de Berg, T.: OMI level 0 to 1b processing and operational aspects, IEEE T. Geosci. Remote, 44, 1380–1397, doi:10.1109/TGRS.2006.872935, 2006. 6708, 6709, 6710

Vandaele, A., Hermans, C., Simon, P., Carleer, M., Colin, R., Fally, S., Mérienne, M., Jenouvrier, A., and Coquart, B.: Measurements of the NO_2 absorption cross-section from 42 000 cm^{-1} to 10 000 cm^{-1} (238–1000 nm) at 220 K and 294 K, J. Quant. Spectrosc. Ra., 59, 171–184, doi:10.1016/S0022-4073(97)00168-4, 1998. 6729

Veefkind, J. P.: CAMELOT Executive Summary, RP-CAM-KNMI-051, 2009. 6707, 6730

Veihelmann, B. and Kleipool, Q.: Reducing Along-Track Stripes in OMI-Level 2 Products, KNMI Technical Document, TN-OMIE-KNMI-785, 2006. 6706

Venter, A. D., Vakkari, V., Beukes, J. P., van Zyl, P. G., Laakso, H., Mabaso, D., Tiitta, P., Josipovic, M., Kulmala, M., Pienaar, J. J., and Laakso, L.: An air quality assessment in the industrialised western Bushveld Igneous Complex, South Africa, S. Afr. J. Sci., 108, 1–10, doi:10.4102/sajs.v108i9/10.1059, 2012. 6715

Vlemmix, T., Piters, A. J. M., Berkhout, A. J. C., Gast, L. F. L., Wang, P., and Levelt, P. F.: Ability of the MAX-DOAS method to derive profile information for NO_2: can the boundary layer and free troposphere be separated?, Atmos. Meas. Tech., 4, 2659–2684, doi:10.5194/amt-4-2659-2011, 2011. 6707

Voors, R., Dobber, M., Dirksen, R., and Levelt, P.: Method of calibration to correct for cloud-induced wavelength shifts in the Aura satellite's Ozone Monitoring Instrument, Appl. Optics, 45, 3652–3658, doi:10.1364/AO.45.003652, 2006. 6709, 6711, 6719

Vountas, M., Rozanov, V., and Burrows, J.: Ring effect: Impact of rotational Raman scattering on radiative transfer in Earth's atmosphere, J. Quant. Spectrosc. Ra., 60, 943–961, doi:10.1016/S0022-4073(97)00186-6, 1998. 6707, 6729

Wayne, R. P.: Chemistry of Atmospheres: An Introduction to the Chemistry of the Atmospheres of Earth, the Planets, and Their Satellites, Oxford University Press, USA, 1991. 6701

AMTD
7, 6699–6742, 2014

WHO: World Health Organization (WHO): Health aspects of air pollution with particulate matter, ozone and nitrogen dioxide. Report on a WHO Working Group, Report on a WHO Working Group, Regional Office for Europe, Bonn, Germany, 13–15 January 2003, EUR/03/5042688, 2003. 6700

Ziemke, J. R., Chandra, S., and Bhartia, P. K.: "Cloud slicing": a new technique to derive upper tropospheric ozone from satellite measurements, J. Geophys. Res.-Atmos., 106, 9853–9867, doi:10.1029/2000JD900768, 2001. 6719

AMTD
7, 6699–6742, 2014

Table 1. The absorption cross-sections used in the DOAS fits for this work.

Species	Reference (SCIATRAN)	Reference (OMI, OMNO2A)	Reference (OMI, Earthshine reference)
NO_2 (220 K)	Vandaele et al. (1998)	Vandaele et al. (1998)	Vandaele et al. (1998)
O_3	Bogumil et al. (1999)	Boersma et al. (2007)	Boersma et al. (2007)
H_2O	Rothman et al. (2009)	Rothman et al. (2005)	Rothman et al. (2005)
Ring	Vountas et al. (1998)	J. F. De Haan (personal communication, 2004)	J. F. De Haan (personal communication, 2004)
Polynomial	3rd order	5th order	3rd order
H_2O (liquid)	N/A	N/A	Pope and Fry (1997)
Sand	N/A	N/A	Richter et al. (2011)

AMTD
7, 6699–6742, 2014

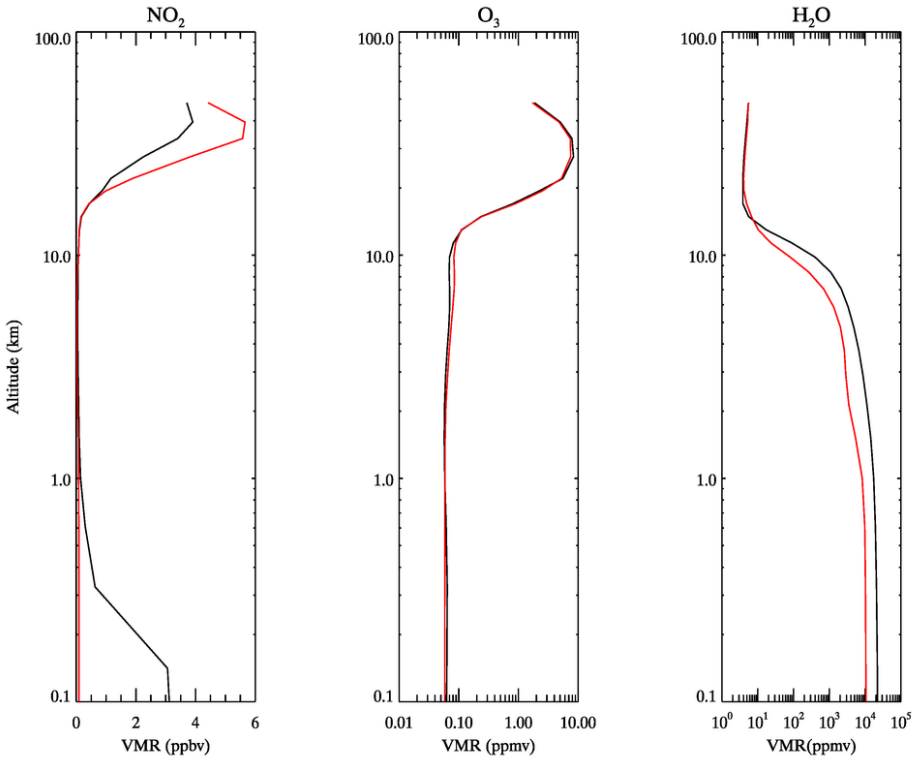

Figure 1. Atmospheric volume mixing ratio (VMR) profiles used in the modelled spectra retrieval for the polluted China (black) and the clean Pacific (red) scenarios. The profiles were taken from Veefkind (2009).

AMTD
7, 6699–6742, 2014

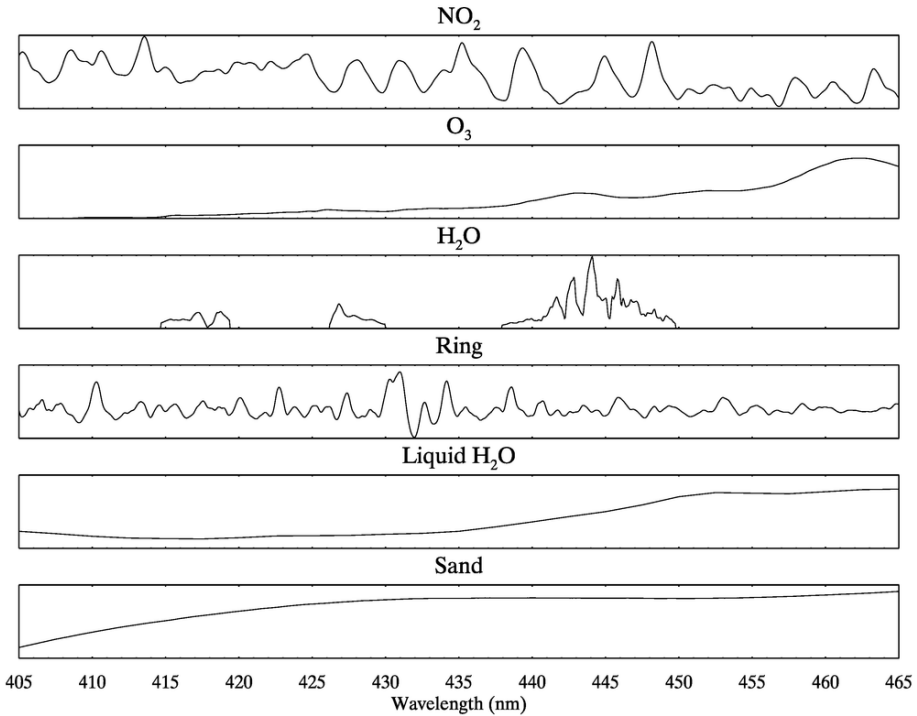

Figure 2. The absorption cross sections used in this work (see Table 1).

AMTD
7, 6699–6742, 2014

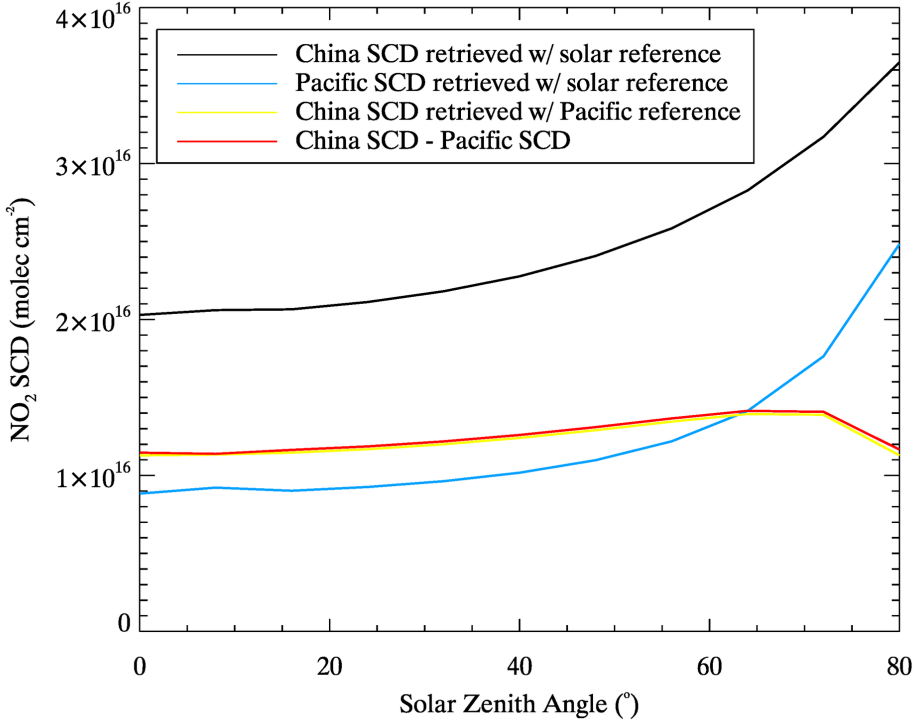

Figure 3. The retrieved NO_2 SCDs from DOAS fitting spectra modelled using SCIATRAN based on the Pacific and Chinese CAMELOT scenarios (Fig. 1) using a range of solar zenith angles (SZA). The red curve indicates the difference between the total SCD of the Pacific and Chinese scenarios directly modelled by SCIATRAN, while the other curves show the SCDs retrieved by using a solar or earthshine reference spectrum in the DOAS fit.

AMTD
7, 6699–6742, 2014

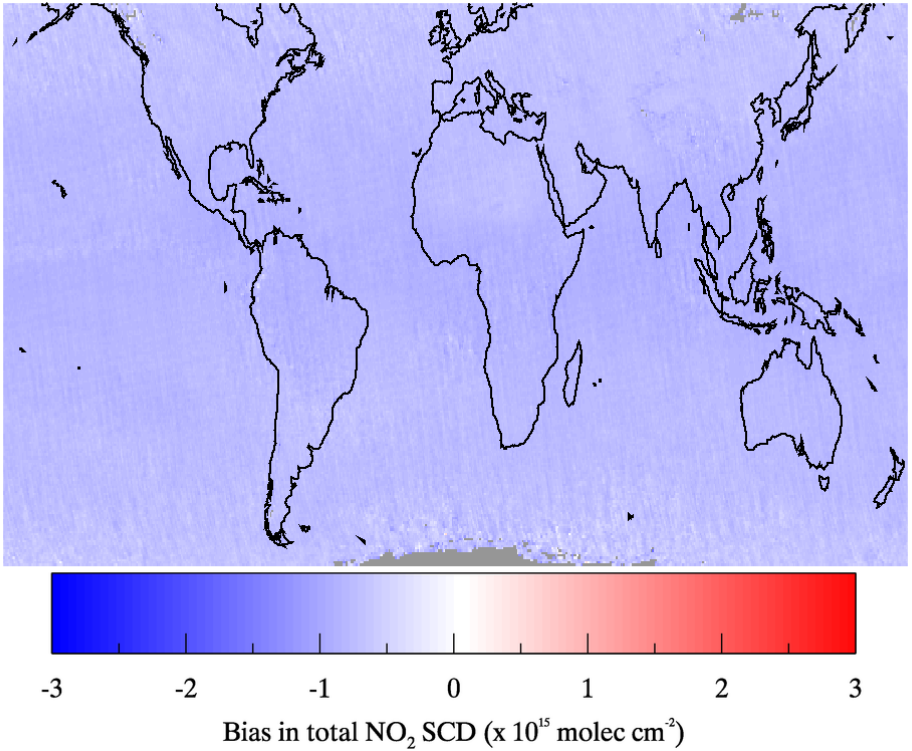

Figure 4. Average total NO_2 SCD bias between the QDOAS-based solar reference retrieval and the OMNO2A algorithm for cloud-free (cloud fraction < 25 %) scenes during June 2005.

AMTD
7, 6699–6742, 2014

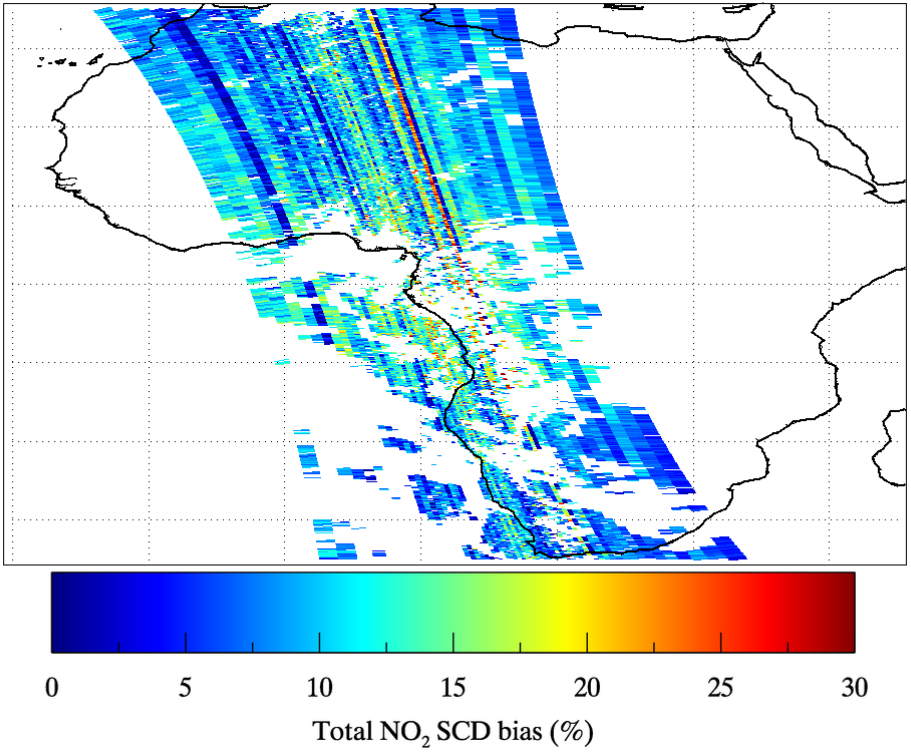

Figure 5. The normalised magnitude of the bias between the total NO_2 SCD retrieved using the OMNO2A algorithm and the QDOAS-based solar reference retrieval. Cloud-free pixels (cloud fraction < 25 %) were compared. The earthshine radiance L1B data was taken from orbit no. 06644 (OML1BRVG).

AMTD
7, 6699–6742, 2014

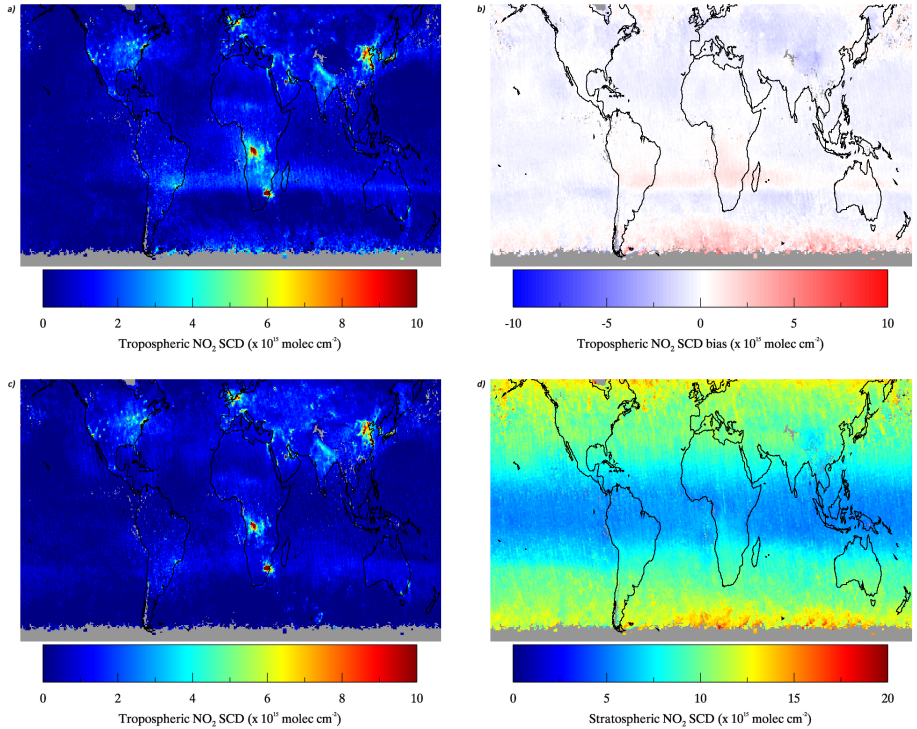

Figure 6. Comparison of average tropospheric NO_2 SCD retrieved during June 2005 using the ESrs-DOAS technique with DOMINO. **(a)** Average tropospheric NO_2 SCD retrieved using an earthshine reference. **(b)** Average bias between earthshine retrieval and DOMINO tropospheric SCD. **(c)** Average tropospheric NO_2 SCD retrieved by DOMINO. **(d)** Average stratospheric NO_2 SCD retrieved by DOMINO.

AMTD
7, 6699–6742, 2014

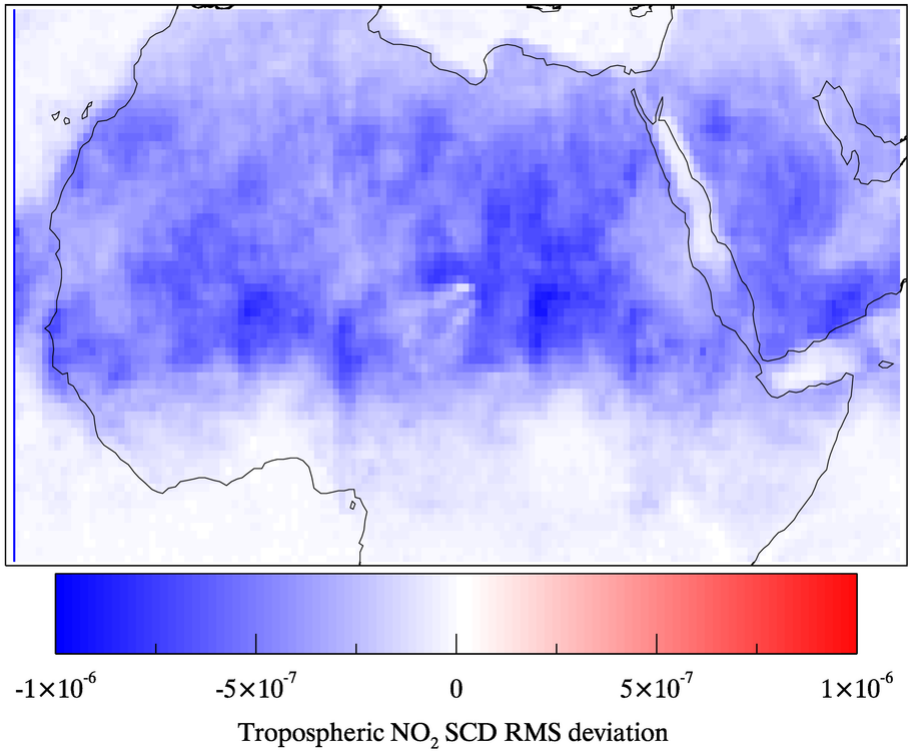

Figure 7. The change in RMS resulting from adding the sand and liquid water absorption cross sections to the earthshine reference DOAS fit. DOAS fits for OMI spectra measured over the Sahara desert during June 2005 were performed using a Pacific earthshine reference with the default OMNO2A cross sections and with the addition of a sand and liquid water cross section (see Table 1).

AMTD
7, 6699–6742, 2014

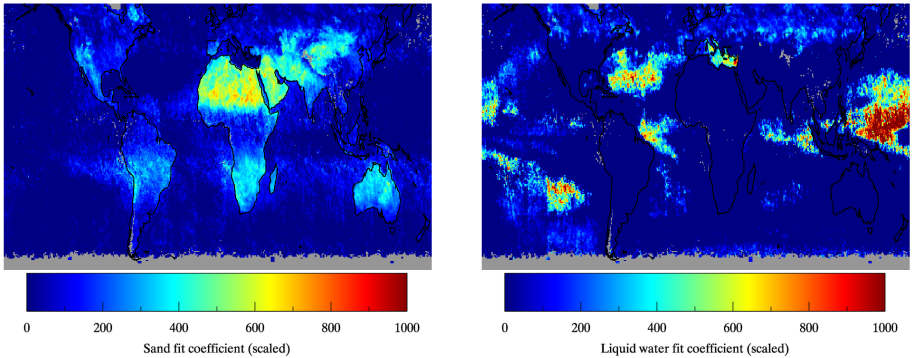

Figure 8. Average tropospheric sand (left) and liquid water (right) fit coefficient retrieved using earthshine reference DOAS during June 2005. Note that only positive SCDs have been plotted, and have been scaled to arbitrary values.

AMTD
7, 6699–6742, 2014

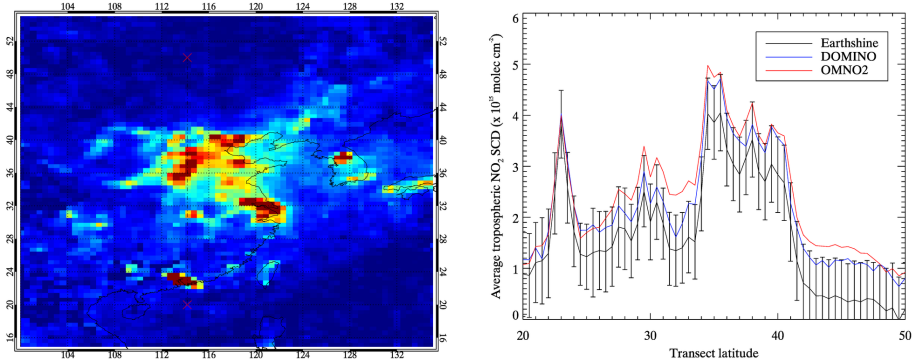

Figure 9. The mean tropospheric NO_2 SCD retrieved over the transect (20–50° N, 114° E) during June 2005. The mean tropospheric SCD retrieved by DOMINO (left, also showing the transect coordinates) was compared with that retrieved using the OMNO2 algorithm and the earthshine reference method (right). The error bars are the mean uncertainty of the SCDs retrieved using an earthshine reference, as calculated by QDOAS (Fayt et al., 2013).

AMTD
7, 6699–6742, 2014

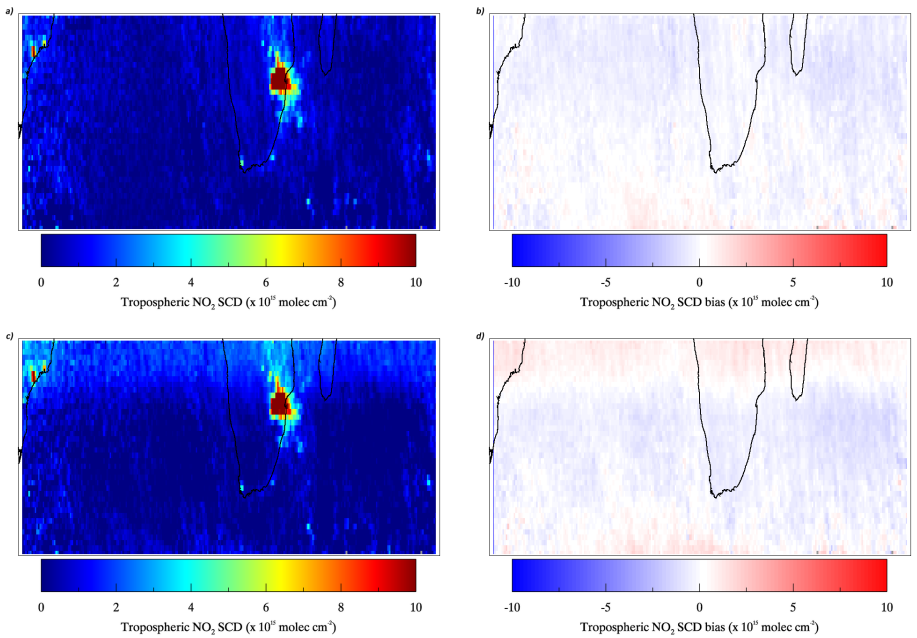

Figure 10. Comparison of tropospheric NO_2 SCDs retrieved over South Africa (20–40° S, 50° W–80° E) using Pacific and South Atlantic reference spectra with DOMINO. **(a)** Average tropospheric NO_2 SCD retrieved using a S. Atlantic earthshine reference. **(b)** Average bias between S. Atlantic earthshine retrieval and DOMINO tropospheric SCD. **(c)** Average tropospheric NO_2 SCD retrieved using a Pacific earthshine reference spectrum. **(d)** Average bias between Pacific earthshine retrieval and DOMINO tropospheric SCD.

AMTD
7, 6699–6742, 2014

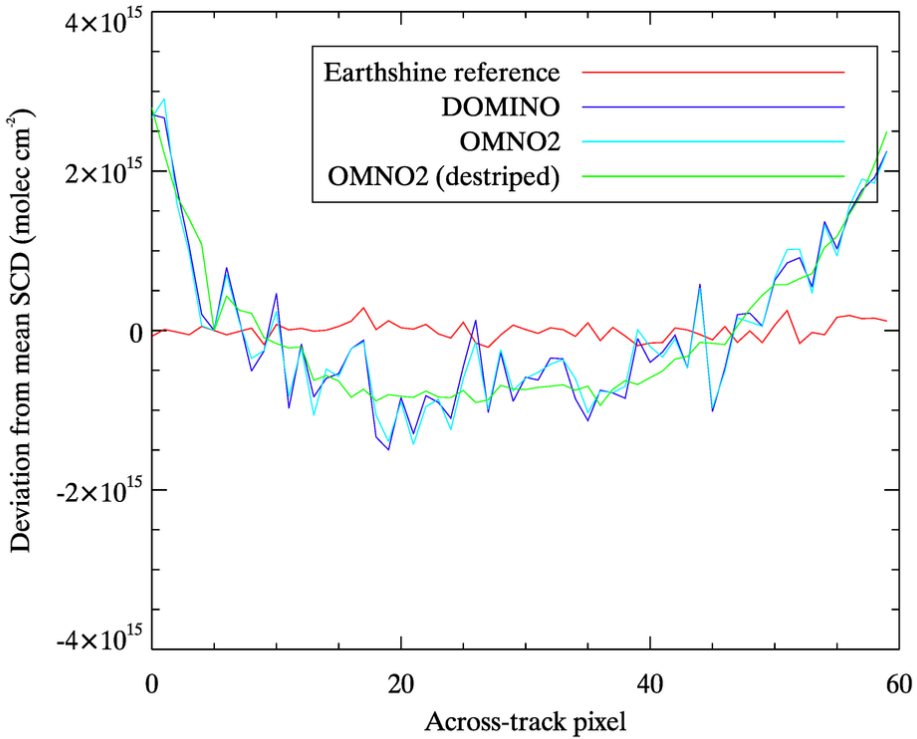

Figure 11. Deviations from the across-track mean NO_2 SCD retrieved by the earthshine reference algorithm and the OMNO2 and DOMINO algorithms. The earthshine radiance L1B and OMNO2/DOMINO L2 data was taken from orbit no. 04741.

AMTD
7, 6699–6742, 2014

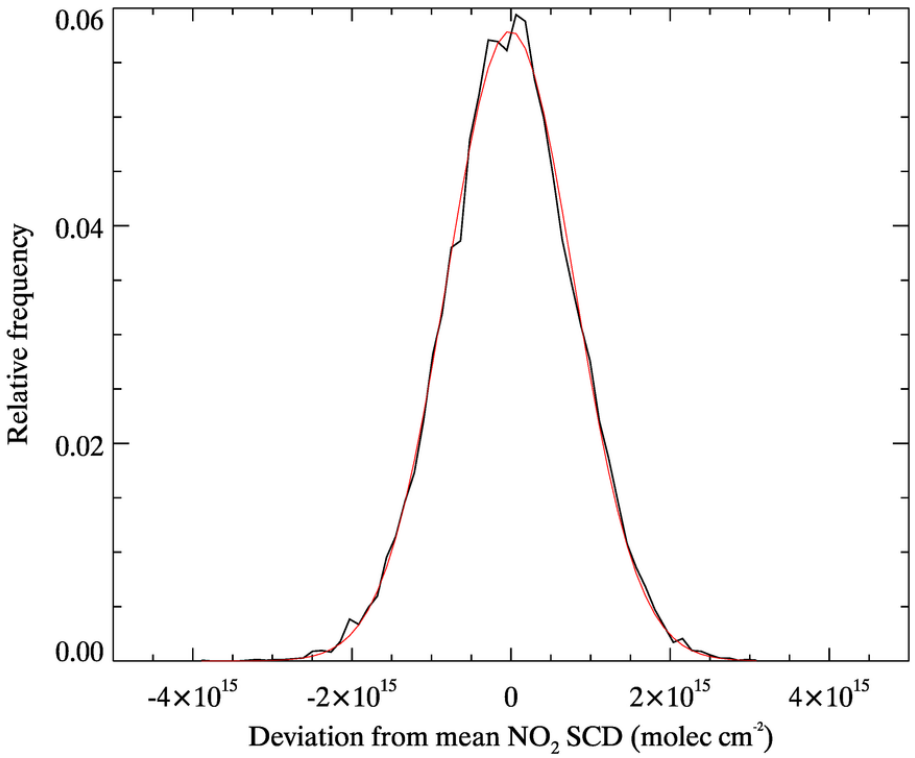

Figure 12. The distribution of the deviations of OMI NO_2 SCDs from the box-mean ($2^\circ \times 2^\circ$) values in the equatorial Pacific region (100–120° W, 10° N–10° S) for June 2005. The SCDs were derived by DOAS fitting OMI spectra using an earthshine reference. The red line shows the fitted Gaussian function.

AMTD
7, 6699–6742, 2014

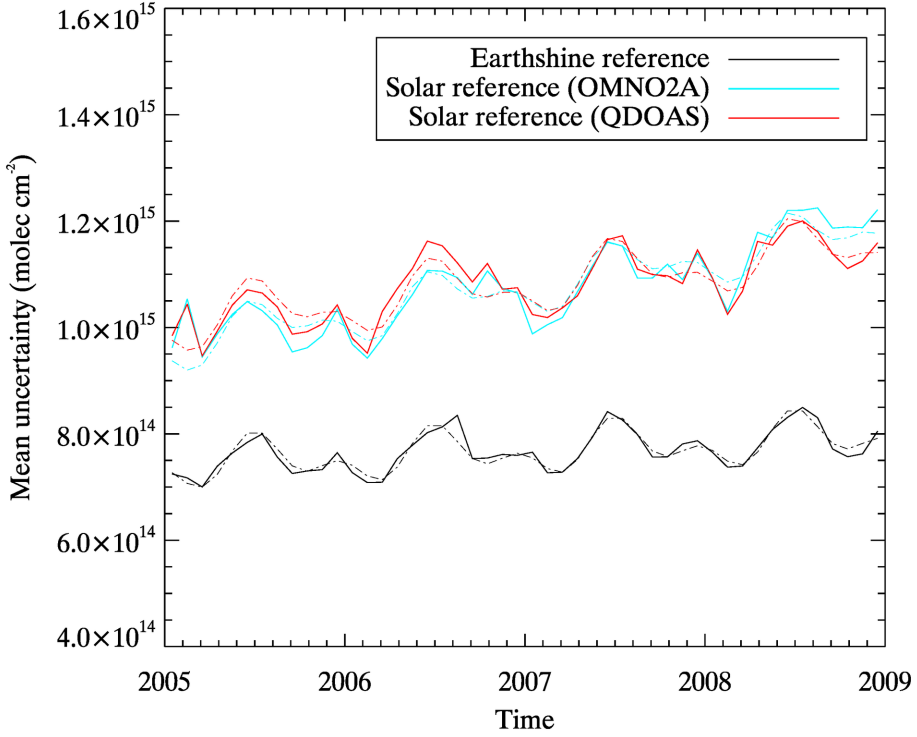

Figure 13. Time series of the monthly mean OMI NO_2 uncertainty between 2005–2008 calculated using the box-mean technique in Fig. 12. The dotted line represents the linear trend and seasonal cycle fitted using regression.

AMTD
7, 6699–6742, 2014